

# 1 Analyze Nucleic Acids Structures and 2 Trajectories with Barnaba.

3 **Sandro Bottaro**<sup>1,2\*</sup>, **Giovanni Bussi**<sup>2\*</sup>, **Giovanni Pinamonti**<sup>2,3</sup>, **Sabine**  
4 **ReiBer**<sup>2</sup>, **Wouter Boomsma**<sup>4</sup>, **Kresten Lindorff-Larsen**<sup>1</sup>

\*For correspondence:

[sandro.bottaro@bio.ku.dk](mailto:sandro.bottaro@bio.ku.dk) (SB); [bussi@sissa.it](mailto:bussi@sissa.it) (GB)

5 <sup>1</sup>Structural Biology and NMR Laboratory, Department of Biology,  
6 University of Copenhagen, Copenhagen, Denmark; <sup>2</sup>International School  
7 for Advanced Studies, Trieste, Italy; <sup>3</sup>Department of Mathematics and  
8 Computer Science, Freie Universität, Berlin, Germany; <sup>4</sup>Department of  
9 Computer Science, University of Copenhagen, Copenhagen, Denmark

---

10  
11 **Abstract** RNA molecules are highly dynamic systems characterized by a  
12 complex interplay between sequence, structure, dynamics, and function.  
13 Molecular simulations can potentially provide powerful insights into the nature of  
14 these relationships. The analysis of structures and molecular trajectories of  
15 nucleic acids can be non-trivial because it requires processing very  
16 high-dimensional data that are not easy to visualize and interpret.  
17 Here we introduce Barnaba, a Python library aimed at facilitating the analysis of  
18 nucleic acids structures and molecular simulations. The software consists of a  
19 variety of analysis tools that allow the user to i) calculate distances between  
20 three-dimensional structures using different metrics, ii) back-calculate  
21 experimental data from three-dimensional structures, iii) perform cluster analysis  
22 and dimensionality reductions, iv) search three-dimensional motifs in PDB  
23 structures and trajectories and v) construct elastic network models (ENM) for  
24 nucleic acids and nucleic acids-protein complexes.  
25 In addition, Barnaba makes it possible to calculate torsion angles, pucker  
26 conformations and to detect base-pairing/base-stacking interactions. Barnaba  
27 produces graphics that conveniently visualize both secondary structure and  
28 dynamics for a set of molecular conformations. Barnaba is available both as a  
29 command-line tool as well as a library, and supports a variety of file formats such  
30 as PDB, dcd and xtc files. Source code, documentation and examples are freely  
31 available at <https://github.com/srnas/barnaba> under GNU GPLv3 license.

---

32

## 33 Introduction

34 Despite their simple four-letters alphabet, RNA molecules can adopt amazingly  
35 complex three-dimensional architectures. RNA structure is often described in  
36 terms of few, simple degrees of freedom such as backbone torsion angles,  
37 sugar puckering, base-base interactions, and helical parameters *Dickerson (1989);*  
38 *Richardson et al. (2008)*. Given a known three-dimensional structure, the cal-  
39 culation of these properties can be performed using available tools such as  
40 MC-annotate *Gendron et al. (2001)*, 3DNA *Lu and Olson (2008)*, fr3D *Sarver et al.*  
41 *(2008)* or DSSR *Lu et al. (2015)*. These software packages make it possible to  
42 calculate a variety of structural properties, but are less suitable for analyzing and  
43 comparing large numbers of structures.

44 The lack of large-scale analysis tools is critical when considering that many RNA  
45 molecules are not static, but highly dynamic entities, and multiple conformations  
46 are required to describe their properties. In Molecular dynamics (MD) simulations,  
47 for example, it is often necessary to analyze several hundreds thousands of  
48 structures. In order to rationalize and generate scientific insights, it is therefore  
49 fundamental to employ specific analysis and visualization tools that can handle  
50 such highly-dimensional data. This need has been long recognized in the field  
51 of protein simulations, leading to the development of several software packages  
52 for the analysis of MD trajectories *Michaud-Agrawal et al. (2011); McGibbon et al.*  
53 *(2015); Tiberti et al. (2015)*. While these software can be in principle used to  
54 analyze generic simulations, they do not support the calculation of nucleic acids-  
55 specific quantities out-of-the box.

56 A limited number of software packages have been developed with the main  
57 purpose of analyzing simulations of nucleic acids. Curves+ *Lavery et al. (2009)*  
58 calculates parameters in DNA/RNA double helices as well as torsion backbone  
59 angles.  $do_{x3dna}$  *Kumar and Grubmüller (2015)* extends the capability of the 3DNA  
60 package to analyze few selected quantities from GROMACS *Abraham et al. (2015)*  
61 MD trajectories. The detection of hydrogen bonds/stacking in simulations and the  
62 identification of motifs such as helices, junctions, loops, etc. can be performed  
63 using the Motif Identifier for Nucleic acids Trajectory (MINT) software *Górska et al.*  
64 *(2015)*.

65 Here we present Barnaba, a Python library to analyze nucleic acids structures  
66 and trajectories. The library contains routines to calculate various structural pa-  
67 rameters (e.g. distances, torsion angles, base-pair and base-stacking detection), to  
68 perform dimensionality reduction and clustering, to back-calculate experimental  
69 quantities from structures and to construct elastic network models. Barnaba  
70 utilizes the capabilities of MDTraj *McGibbon et al. (2015)* for reading/writing tra-  
71 jectory files, and thus supports many different formats, including PDB, dcd, xtc,  
72 and trr.

73 In this paper we show the capabilities of Barnaba by analyzing a long MD  
74 simulation of an RNA stem-loop structure. We first calculate distances from a  
75 reference frame. Second, we consider a subset of dihedral angles and compare  
76  $^3J$  scalar couplings calculated from simulations with nuclear magnetic resonance  
77 (NMR) data. We then perform a cluster analysis of the trajectory, identifying  
78 a number of clusters that are visualized using a dynamic secondary structure  
79 representation. Finally, we search for structural motifs similar to cluster centroids  
80 in the entire protein data bank (PDB) database. In addition, we show how to  
81 construct an elastic network model (ENM) of RNA molecules and protein-nucleic  
82 acid complexes with Barnaba, and how to use it to estimate RNA local fluctuations.

## 83 Results

84 We present the different features of Barnaba by analyzing the reversible folding  
85 simulation of an RNA 14-mers with sequence GGCACUUCGGUGCC performed by Tan  
86 et al. *Tan et al. (2018)*. Experimentally, this sequence is known to form an A-form  
87 stem composed by 5 consecutive Watson-Crick base-pairs, capped by a UUCG  
88 tetraloop (Fig. 1A).

### 89 RMSD, eRMSD calculation and detection of base-base interactions.

90 First, we calculate the distance of each frame in the simulation from the ref-  
91 erence experimental structure (PDB code 2KOC *Nozinovic et al. (2010)*). Fig.1B  
92 shows the time series of heavy-atom root mean squared distance (RMSD) after  
93 optimal superposition *Kabsch (1976)*. During this simulation, multiple folding  
94 events occur: we thus observe both structures close to the reference as well as  
95 unfolded/misfolded ones.

96 We identify the base-base interactions in each frame using the annotation  
97 functionality in Barnaba (see Methods). Structures where the stem is completely  
98 formed together with the native trans sugar-Watson (tSW) interaction between  
99 U6-G9 in the loop are shown in red. Blue points indicate structures in which all  
100 base-pairs in the stem are present, but not in the loop. All the other structures are  
101 colored in gray. From the histogram in Fig. 1B it can be seen that  $\text{RMSD} < 0.23\text{nm}$   
102 roughly corresponds to native-like structures. A second sharp peak around  $0.3\text{nm}$   
103 corresponds to structures in which only the stem is correctly formed. All other  
104 conformations have RMSD larger than  $0.6\text{nm}$ .

105 One of the peculiar feature of Barnaba is the possibility to calculate the eRMSD  
106 *Bottaro et al. (2014)*. The eRMSD only considers the relative arrangements be-  
107 tween nucleobases in a molecule, and quantifies the differences in the interaction  
108 network between two structures. In this perspective, eRMSD is similar to the  
109 Interaction Fidelity Network *Parisien et al. (2009)* that quantifies the discrepancy  
110 in the set of base-pairs and base-stacking interactions. The eRMSD, however,  
111 is a continuous, symmetric, positive definite metric distance that satisfies the

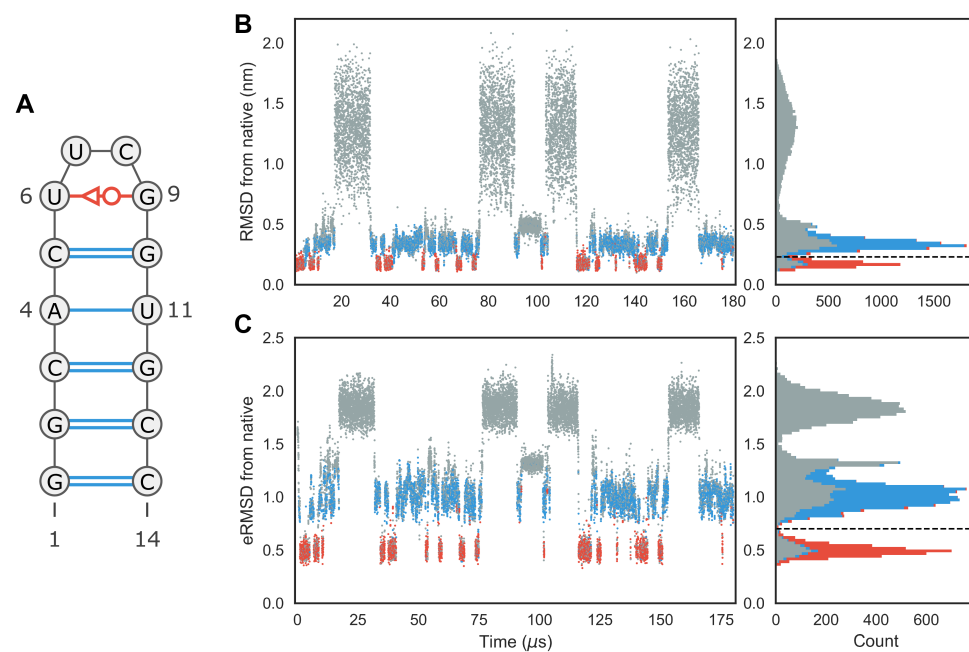


**Figure 1.** **A)** Secondary structure representation of the UUCG stem-loop. Watson-Crick base-pairs are shown in blue, trans Sugar-Watson base-pair between U6 and G9 is shown in red. **B)** RMSD from native over time of the UUCG simulation. The corresponding histogram is shown in the right panel. The dashed line at RMSD=0.23nm separates native-like from non-native-like structures. The colors indicate the presence of native base-base interactions, as shown in the secondary structure representation. Structures where all Watson-Crick interactions in the stem and the trans Sugar-Watson base-pair in loop is formed are shown in red. Blue indicates structures where only the stem is formed. All other conformations are shown in gray. **C)** eRMSD from native structure over time. Color scheme is identical to panel **B**. Dashed line at eRMSD=0.7 separates native-like from non-native conformations.

112 triangular inequality. Additionally, it does not require detection of the interactions  
113 (annotation) and is hence particularly well suited for analyzing MD trajectories  
114 and unstructured RNA molecules. Fig.1C shows the eRMSD from native for the  
115 UUCG simulation. We notice that, similarly to the RMSD case, the histogram  
116 displays three main peaks. In this case the correspondence between peaks and  
117 structures can be readily identified: when  $eRMSD < 0.7$  native stem and loop  
118 are formed, if  $0.7 < eRMSD < 1.3$ , stem is formed but the loop is in a non-native  
119 configuration. Other structures typically have  $eRMSD > 1.3$ . We observe that the  
120 separation between the two main peaks (native structure, red, and native stem,  
121 blue) is sharper in Fig.1C, confirming that eRMSD is more suitable than RMSD to  
122 distinguish structure with different base pairings **Bottaro et al. (2014)**.

123 Note that a significant number of low-RMSD/eRMSD structures lack one or  
124 more native base-pair interactions, and are therefore shown in gray. This is  
125 because the detection of base-base interactions critically depends on a set of  
126 geometrical parameters (e.g. distance, base-base orientation, etc.) that were  
127 calibrated on high-resolution structures. The criteria used in Barnaba (as well as  
128 the ones employed in other annotation tools) may not always be accurate when  
129 considering intermediate states and partially formed interactions that are often  
130 observed in molecular simulations.

### 131 **Torsion angle and $^3J$ scalar coupling calculations**

132 Another important class of structural parameters is torsion angles. Similarly to  
133 other software, Barnaba contains routines to calculate backbone torsion angles  
134 ( $\alpha, \beta, \gamma, \delta, \epsilon, \zeta$ ), the glycosidic angle  $\chi$ , and the pseudorotation sugar parameters  
135 **Altona and Sundaralingam (1972)**.

136 In Fig. 2, left panels we plot the probability distributions of four angles ( $\beta, \gamma, \delta$   
137 and  $\epsilon$ ) for three different residues: U6, U7, and G9. We can see from the dis-  
138 tribution of  $\gamma$  angles that U6 and U7 mainly populate the *gauche*<sup>+</sup> rotameric  
139 state ( $0^\circ < \gamma \leq 120^\circ$ ), while G9 significantly populates the *trans* state as well  
140 ( $120^\circ < \gamma \leq 240^\circ$ ). Differences in rotameric states can be also seen from the  
141 distribution of  $\delta$  angles (C2'/C3'-endo) and  $\epsilon$ , that is related to BI/BII states.

142 In this example we chose these specific torsion angles because their distribu-  
143 tion is related to available  $^3J$  couplings experimental data from nuclear magnetic  
144 resonance (NMR) spectroscopy. The magnitude of  $^3J$  coupling depends on the dis-  
145 tance between atoms connected by three bonds, and thus on the corresponding  
146 dihedral angle distribution. The dependence between angle  $\theta$  and coupling  $^3J$   
147 can be calculated via Karplus equations  $^3J = A \cos^2(\theta + \phi) + B \cos(\theta + \phi) + C$ , where  
148  $A, B, C$  are empirical parameters. Couplings corresponding to different angles can  
149 be calculated with Barnaba. H1'-H2', H2'-H3', H3'-H4' (sugar conformation), H5'-P,  
150 H5''-P, C4-P ( $\beta$ ), H4'-H5', H4'-H5'' ( $\gamma$ ), H3-P(+1), C4-P(+1) ( $\epsilon$ ), H1'-C8/C6, and H1'-C4/C2  
151 ( $\chi$ ). The complete list of Karplus parameters are reported in the Methods section.

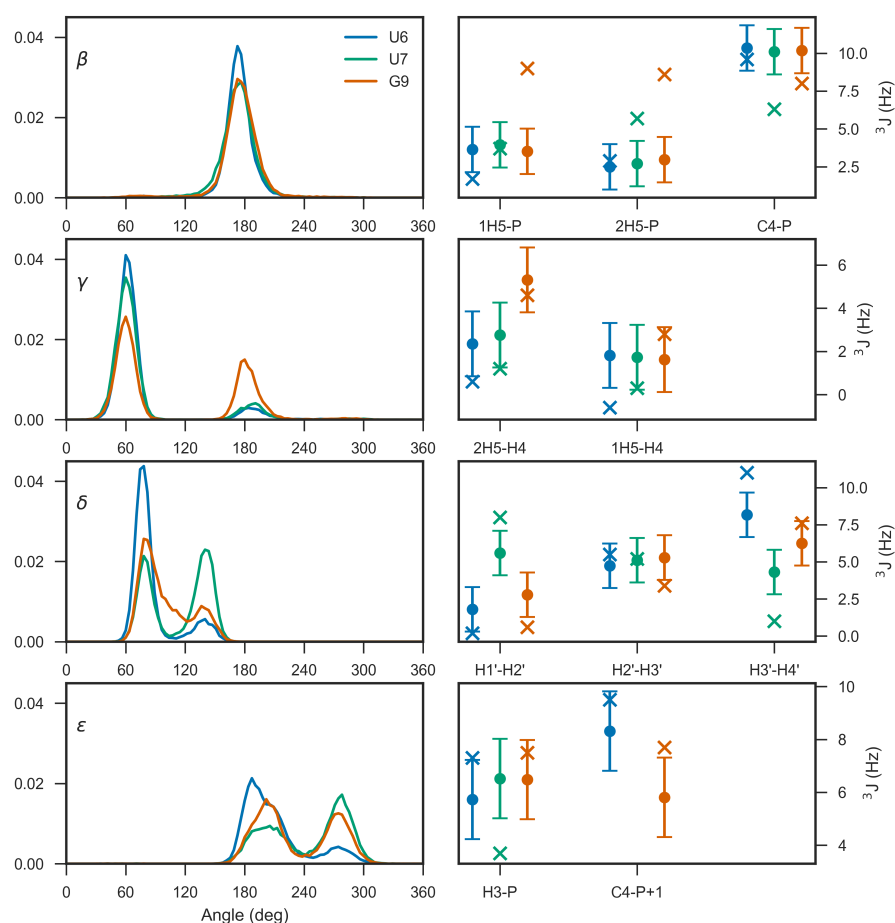


**Figure 2.** Left panels: Torsion angle distribution for  $\beta, \gamma, \delta$  and  $\epsilon$  in residues U6, U7, and G9. Right panels show the experimental  $^3J$  couplings (crosses) and the calculated value from simulation (dots). The error bars indicate the standard error of the mean calculated over 4 blocks.

152 Fig. 2, right panel, shows the back-calculated average  $^3J$  couplings and the  
 153 corresponding experimental value reported in *Nozinovic et al. (2010)*. Note that  
 154 in some cases experiments and simulations do not agree: this is because the  
 155 simulation was performed at different temperatures using a simulated tempering  
 156 protocol, and therefore the comparison between simulations and experiments is  
 157 here made for illustrative purposes only. Significant discrepancies could originate  
 158 from errors introduced by the Karplus equations, that can be as large as 2Hz  
 159 *Bottaro et al. (2018)*.

## 160 Cluster analysis

161 The structures within a trajectory can be grouped into clusters of mutually similar  
 162 conformations, to understand which different states are visited and how often.  
 163 Here, we consider the same trajectory of the UUCG tetraloops described above,

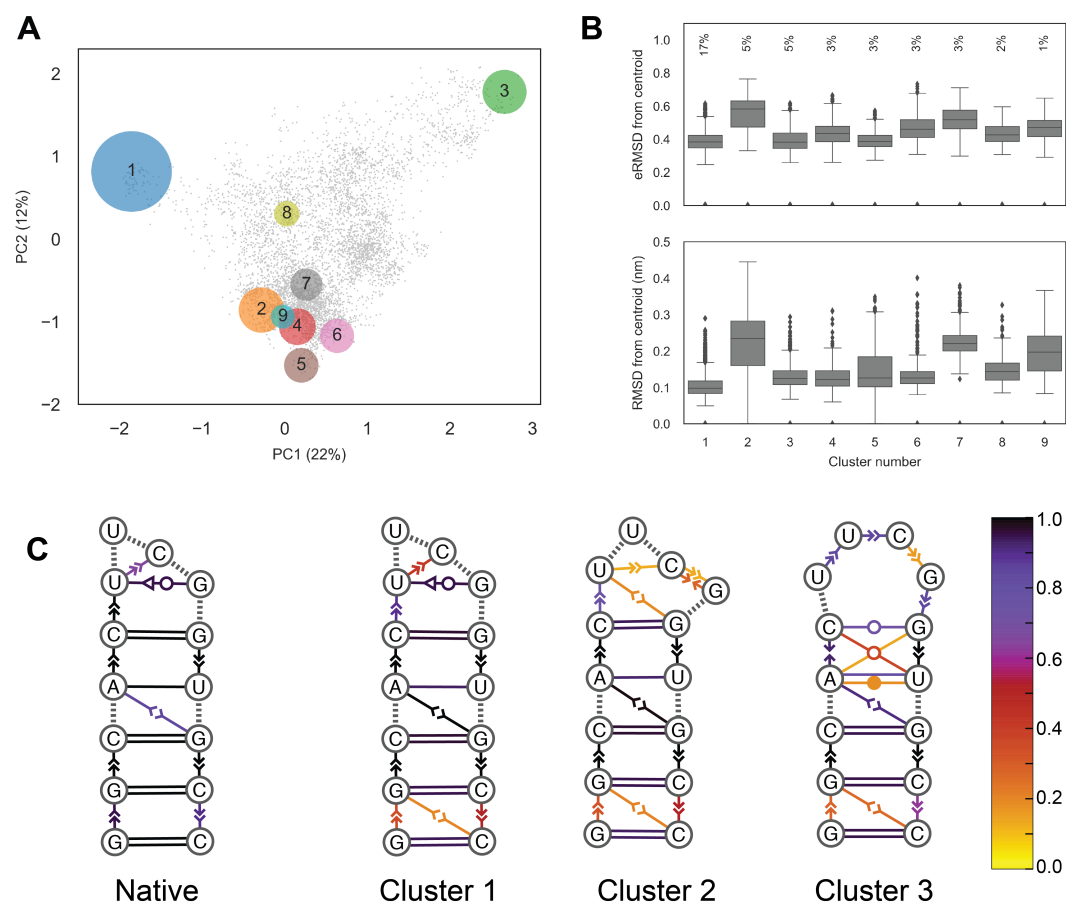


**Figure 3.** Example of a cluster analysis on the UUCG stem-loop trajectory. **A**) principal component analysis on the collection of G-vectors *Bottaro and Lindorff-Larsen (2017)*. Each circle corresponds to a cluster, gray dots show unassigned structures. Circles are centered in the centroid positions, and the radii are proportional to the square root of the the population. The percentage of explained variance of the first two components is indicated on the axes. **B**) Box-plots reporting eRMSD (top) and RMSD (bottom) from cluster centroids. Lower/upper hinges correspond to the first and third quartiles, while whiskers indicate lowest/highest data within 1.5 interquartile range. Data beyond the end of the whiskers are shown individually. The percentages indicate the cluster population. **C**) Dynamic secondary structure representation of the 20 native NMR conformers (PDB 2KOC) and of the first three clusters. The secondary structure annotation follows the Leontis-Westhof classification. The color scheme shows the number of frames within a cluster for which the interaction is formed.



164 and removed all the unfolded structures, i.e. structures with eRMSD from native  
165 larger than 1.5 ( $\approx$  6000 out of 20000). For clustering we use the DBSCAN *Ester et al.*  
166 (1996) algorithm with  $\epsilon = 0.45$  and min samples=70 *Bottaro and Lindorff-Larsen*  
167 (2017). Figure 3A shows the trajectory projected onto the first two components  
168 of a principal component analysis done on the collection of G-vectors *Bottaro*  
169 *and Lindorff-Larsen (2017)*. Circles show the resulting 9 clusters, whose radius is  
170 proportional to the square root of their size. Structures that were not assigned to  
171 any cluster (5500) are shown as gray dots. For each cluster we identify its centroid,  
172 here defined as the structure with the lowest average distance from all other  
173 cluster members.

174 Ideally, clusters should be compact enough so that the centroid can be con-  
175 sidered as a representative structure. This information is shown in the box-plot  
176 in Fig. 3B, that reports the distances (eRMSD and RMSD, as labeled) between  
177 centroids and cluster members. At the same time, structures within clusters are  
178 not all identical one to the other. In order to visualize the intra-cluster variability  
179 we have found it useful to introduce a “dynamic secondary structure” representa-  
180 tion. In essence, we detect base-stacking/base-pair interactions in all structures  
181 within a cluster, and calculate the fraction of frames in which each interaction is  
182 present. The population of each interaction is shown by coloring the standard  
183 secondary-structure representation, as shown in Fig.3C. We can see that the first  
184 three clusters correspond to three different tetraloop structures. In cluster 1, the  
185 U6-G9 tSW base pair is present, together with the U6-C8 stacking typical of the  
186 native UUCG tetraloop structure. In cluster 2, no U6-G9 base-pair is present, while  
187 in cluster 3 we observe stacking between U6-U7-C8-G9, as also described in the  
188 next section. In all clusters the population of the terminal base-pairs and stacking  
189 is lower than one, indicating the presence of base-fraying.

190 In our experience, cluster analysis is useful to understand and visualize quali-  
191 tatively the different type of structures in a simulation. In many practical cases,  
192 however, the number of clusters and their population may differ depending on  
193 the employed clustering algorithm and associated parameters. Clustering may  
194 not even be meaningful when considering highly unstructured systems such as  
195 long single-stranded nucleic acids lacking secondary structures *Chen et al. (2012)*.

## 196 **Motif search**

197 Barnaba can be used to search for structural motifs in a PDB file or trajectory  
198 using the eRMSD distance. In the following example, we illustrate this feature  
199 by taking the centroids of the first three clusters described above and search for  
200 similar structures within the PDB database. In order to focus on the loop structure,  
201 rather than on stem variability, we consider the tetraloop and the two closing  
202 base-pairs for the search (residues 4-11 in Fig.1). The search is performed  
203 against all RNA-containing structures in the PDB database (retrieved May 4th,



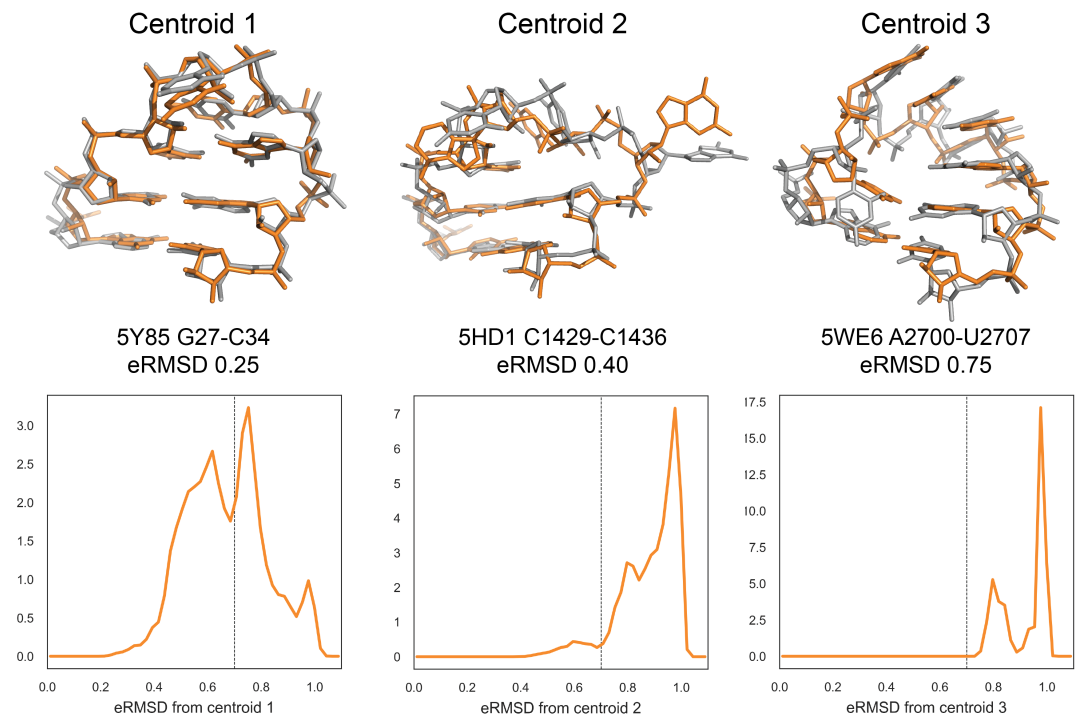


**Figure 4.** Motif search in PDB database. Top panels: centroids of the first three clusters (in gray) superimposed on the closest structures from the PDB database (orange). eRMSD between centroid and the best match are indicated, together with the associated PDB code. Bottom panels: eRMSD distribution between centroid and substructures from PDB database. Note that different distributions are obtained for different clusters, meaning that the eRMSD threshold varies depending on the motif. Distances larger than eRMSD=1 are not reported. The eRMSD threshold at 0.7 (centroid 1,2) and 0.9 (centroid 3) is indicated as a dashed line.

204 2018, resolution 3.5Å or better). The entire database consists of 3067 X-ray, 652  
205 NMR and 177 cryo electron-microscopy (EM) structures. Note that the search is  
206 purely based on geometry, without restriction on the sequence.

207 Figure 4, top panels, shows the cluster centroids (gray) and the closest motif  
208 match, i.e. the lowest eRMSD substructure in the PDB database (orange). The  
209 eRMSD between the cluster centroid and the best match are indicated, together  
210 with the associated PDB code. Centroid 1 corresponds to the canonical UUCG  
211 tetraloop structure, with the signature tSW interaction between U6-G9 and G9 in  
212 syn conformation. Note that the eRMSD between centroid and best match is small  
213 (0.25), indicating that simulated and experimental structures are highly similar.  
214 Cluster 2 corresponds to a structure in which the stem is formed, C8 is stacked  
215 on top of U6 and G9 is bulged out. Centroid 3 features four consecutive stacking  
216 between U6-U7-C8-G9. Note that this latter structure is remarkably similar to the  
217 4-stack loop described in *Bottaro and Lindorff-Larsen (2017)*.

218 As a rule of thumb, we consider as significant matches structures below 0.7  
219 eRMSD, but there are cases in which it is worth considering structures in the  
220 0.7-1.0 eRMSD range as well. More generally, it is useful to consider the histogram  
221 of all fragments with eRMSD below 1, as shown in Fig. 4, bottom panels. This type  
222 of analysis makes it possible to identify a good threshold value, in correspondence  
223 to minima in the probability distributions. For example, there are no structures  
224 in the PDB with eRMSD lower than 0.7 for centroid 3. In this case, a value of 0.9  
225 should be used instead.

226 In this example we performed a simple search of single-stranded RNA motifs.  
227 Barnaba also allows for searches with more complex motifs composed by two  
228 strands such as K-turns and sarcin-ricin motifs. Additionally, it can allow for  
229 inserted bases, thereby identifying structural motifs with one or more bulged-out  
230 bases.

## 231 Elastic Network Models

232 Elastic Network Models (ENMs) are minimal computational models able to capture  
233 the dynamics of macromolecules at a small computational cost. They assume that  
234 the system can be represented as a set of beads connected by harmonic springs,  
235 each having rest length equal to the distance between the two beads it connects,  
236 in a reference structure (usually, an experimental structure from the PDB). First  
237 introduced to analyze protein dynamics *Tirion (1996)*, ENMs are also applicable  
238 to structured RNA molecules *Bahar and Jernigan (1998)*; *Setny and Zacharias*  
239 *(2013)*; *Zimmermann and Jernigan (2014)*. Barnaba contains routines to construct  
240 ENM of nucleic acids and proteins, and, as unique feature, makes it possible  
241 to calculate fluctuations between consecutive C2-C2 atoms. In a previous work  
242 *Pinamonti et al. (2015)*, we have shown this quantity to correlate with flexibility  
243 measurements performed with selective 2-hydroxyl acylation analyzed by primer

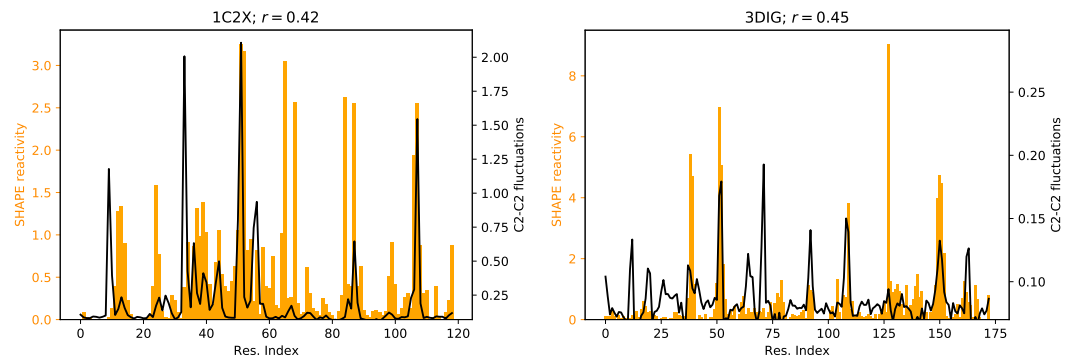


**Figure 5.** C2-C2 fluctuations as predicted by the ENM of Lysine riboswitch (right panel) and 5S rRNA (left panel). SHAPE reactivity data from *Hajdin et al. (2013)* are shown for comparison. Pearson correlation coefficient  $r$  between SHAPE data and ENM-predicted fluctuations is also indicated.

244 extension (SHAPE) experiments *Merino et al. (2005)*. Here, we show an example  
245 of ENM analysis on two RNA molecules: the 174-nucleotide sensing domain of the  
246 *Thermotoga maritima* lysine riboswitch in the lysine-bound state (PDB ID: 3DIG),  
247 and the *Escherichia coli* 5S rRNA (PDB ID: 1C2X). We construct an all-atom ENM  
248 (AA-ENM), where each heavy atom is a bead, together with a cutoff radius of 7 Å.  
249 In figure 5 we show the flexibility of the RNA molecules as predicted by the ENM  
250 (black), that can be qualitatively compared with the measured SHAPE reactivity  
251 *Hajdin et al. (2013)* (orange).

252 The implementation of the ENM in Barnaba employs the sparse matrix package  
253 available in Scipy, that allows for significant speed-ups compared to the dense-  
254 matrix implementation (Fig. 6). This, combined with the significant memory saving  
255 granted by sparse matrices representation, makes it possible to easily compute  
256 the vibrational modes and the local flexibility of large RNA systems such as a  
257 ribosomal structures using a limited amount of computer resources.

## 258 Discussion

259 Many RNA molecules are highly dynamical entities that undergo conformational  
260 rearrangements during function. For this reason, it is becoming increasingly im-  
261 portant to develop tools to analyze not only single structures, but also trajectories  
262 (ensembles) obtained from molecular simulations. In this paper we introduce a  
263 software to facilitate the analysis of nucleic acids simulations. The program, called  
264 Barnaba, is available both as a Python library as well as a command line tool. The  
265 output of the program is such that it can be easily used to calculate averages  
266 and probability distributions, or conveniently used as input to the many existing  
267 plotting and analysis libraries (e.g. Matplotlib, SKlearn) available in Python.

268 Barnaba consists of a number of functions: some of them implement standard  
269 calculations (RMSD, torsion angles, base-pairs and base-stacking detection). A

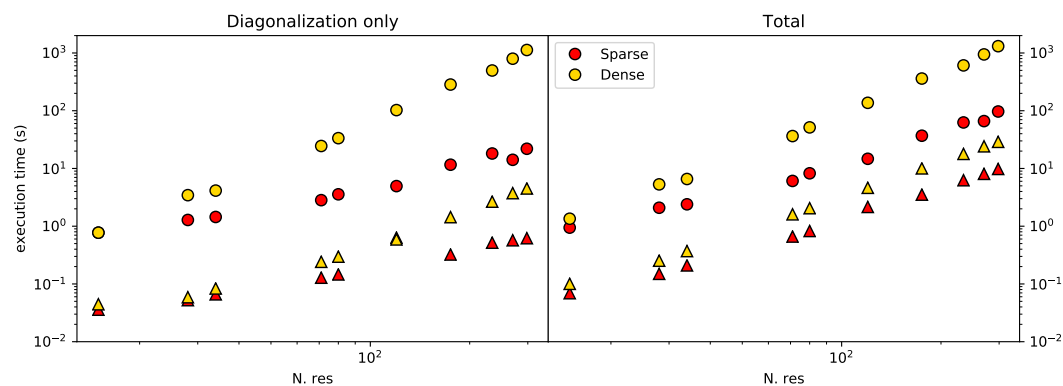


**Figure 6.** Execution time for the ENM calculation using sparse matrices (yellow) or dense matrices (red), as a function of the number of residues in the RNA molecule. Results are shown both for sugar-base-phosphate (SBP) ENM (triangles) and all-atom-ENM (AA-ENM) (circles), as defined in *Pinamonti et al. (2015)*. Left panel shows the time for the interaction matrix diagonalization only, right panel shows the total time including the calculation of C2-C2 fluctuations.

270 unique feature of Barnaba is the possibility to calculate the eRMSD. This metric  
271 has been successfully employed in several contexts: for analyzing MD simula-  
272 tions *Kuhrova et al. (2016)*, as a biasing collective variable in enhanced sampling  
273 simulations *Bottaro et al. (2016)*; *Yang et al. (2017)*, to construct Markov State  
274 models *Pinamonti et al. (2017)* and to cluster RNA tetraloop structures *Bottaro*  
275 *and Lindorff-Larsen (2017)*. In this paper we show the usefulness of this metric  
276 to monitor simulations over time, to perform cluster analysis and to search for  
277 structural motifs within trajectories/structures. This last feature can be extremely  
278 useful to experimental structural biologists, as it makes it possible to efficiently  
279 search for arbitrary query motifs within the entire PDB database.

280 Another unique feature of Barnaba is the possibility to back-calculate  $^3J$  scalar  
281 couplings from structures. This calculation is *per se* extremely simple. However, it  
282 can be difficult to obtain from the literature the different sets of Karplus param-  
283 eters, and the calculation of the corresponding dihedral angles is error-prone.

284 Finally, Barnaba contains a routine to construct ENMs of nucleic acid and  
285 protein systems and complexes. This is a useful, fast and computationally cheap  
286 tool to predict the local dynamical properties of biomolecules, as well as the chain  
287 flexibility of RNA molecules.

## 288 **Methods and Materials**

### 289 **Implementation and availability**

290 Barnaba is a Python library and command line tool. It requires Python 2.7  
291 or > 3.3, Numpy, and Scipy libraries. Additionally, Barnaba requires MDTraj  
292 (<http://mdtraj.org/>) for manipulating structures and trajectories. Source code

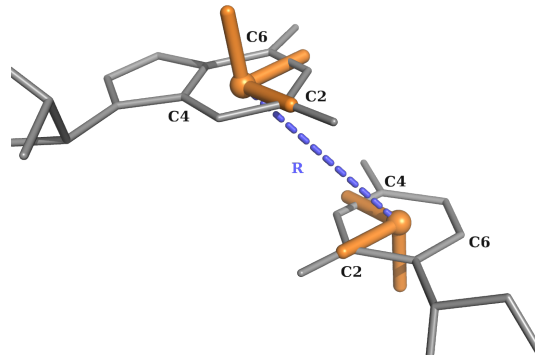


**Figure 7.** Definition of the local coordinate systems and of the vector  $\mathbf{R}$  for purines and pyrimidines.

293 is freely available at <https://github.com/srnas/barnaba> under GNU GPLv3 license.  
294 The github repository contains documentation as well as a set of examples.

### 295 **Relative position and orientation of nucleobases**

296 For each nucleotide, a local coordinate system is set up in the center of C2, C4, and  
297 C6 atoms. The x-axis points toward the C2 atom, and the y-axis in the direction  
298 of C4 (C/U) or C6 (A/G). The origin of the coordinates of nucleobase  $j$  in the  
299 reference system constructed on base  $i$  is the vector  $\mathbf{R}_{ij} = \{x_{ij}, y_{ij}, z_{ij}\}$ . Note that  
300  $|\mathbf{R}_{ij}| = |\mathbf{R}_{ji}|$  but  $\mathbf{R}_{ij} \neq \mathbf{R}_{ji}$ . The  $\mathbf{R}_{ij}$  is central in the definition of the eRMSD metric  
301 and of the annotation strategy described below.

### 302 **eRMSD**

303 The eRMSD is a contact-map based distance, with the addition of a number of  
304 features that make it suitable for the comparison of nucleic acids structures. We  
305 briefly describe here the procedure, originally introduced in *Bottaro et al. (2014)*.  
306 Given a three-dimensional structure  $\alpha$ , one calculates  $\mathbf{R}_{ij}^\alpha$  for all pairs of bases in a  
307 molecule. The position vectors are then rescaled as follows:

$$\tilde{\mathbf{r}}_{ij}^\alpha = \left( \frac{x_{ij}^\alpha}{a}, \frac{y_{ij}^\alpha}{a}, \frac{z_{ij}^\alpha}{b} \right) \quad (1)$$

308 with  $a = 5\text{\AA}$  and  $b = 3\text{\AA}$ . The rescaling effectively introduces an ellipsoidal  
309 anisotropy that is peculiar to base-base interactions. Given two structures,  $\alpha$  and  
310  $\beta$ , consisting of  $N$  residues, the eRMSD is calculated as

$$e\text{RMSD} = \sqrt{\frac{1}{N} \sum_{i,j} |\mathbf{G}(\tilde{\mathbf{r}}_{ij}^\alpha) - \mathbf{G}(\tilde{\mathbf{r}}_{ij}^\beta)|^2} \quad (2)$$

311  $\mathbf{G}$  is a non-linear function of  $\tilde{\mathbf{r}}$  defined as:

$$\mathbf{G}(\tilde{\mathbf{r}}) = \begin{pmatrix} \sin(\gamma\tilde{r}) \frac{\tilde{r}_x}{\tilde{r}} \\ \sin(\gamma\tilde{r}) \frac{\tilde{r}_y}{\tilde{r}} \\ \sin(\gamma\tilde{r}) \frac{\tilde{r}_z}{\tilde{r}} \\ 1 + \cos(\gamma\tilde{r}) \end{pmatrix} \times \frac{\Theta(\tilde{r}_{\text{cutoff}} - \tilde{r})}{\gamma} \quad (3)$$

312 where  $\gamma = \pi/\tilde{r}_{\text{cutoff}}$  and  $\Theta$  is the Heaviside step function. Note that the function  $\mathbf{G}$   
313 has the following desirable properties:

- 314 1.  $|\mathbf{G}(\tilde{\mathbf{r}}^\alpha) - \mathbf{G}(\tilde{\mathbf{r}}^\beta)| \approx |\tilde{\mathbf{r}}^\alpha - \tilde{\mathbf{r}}^\beta|$  if  $\tilde{r}^\alpha, \tilde{r}^\beta \ll \tilde{r}_{\text{cutoff}}$ .
- 315 2.  $|\mathbf{G}(\tilde{\mathbf{r}}^\alpha) - \mathbf{G}(\tilde{\mathbf{r}}^\beta)| = 0$  if  $\tilde{r}^\alpha, \tilde{r}^\beta \geq \tilde{r}_{\text{cutoff}}$ .
- 316 3.  $\mathbf{G}(\tilde{\mathbf{r}})$  is a continuous function.

317 The cutoff value is set to  $\tilde{r}_{\text{cutoff}} = 2.4$ .

### 318 Annotation

319 A pair of bases  $i$  and  $j$  is considered for annotation only if  $|\tilde{\mathbf{r}}_{ij}| < 1.7$  and  $|\tilde{\mathbf{r}}_{ji}| < 1.7$ .

320 **Stacking.** The criteria for base-stacking are the following:

$$(|z_{ij}| \text{ and } |z_{ji}| > 2\text{\AA}) \text{ and } (\rho_{ij} \text{ or } \rho_{ji} < 2.5\text{\AA}) \text{ and } (|\theta_{ij}| < 40^\circ) \quad (4)$$

321 here,  $\rho_{ij} = \sqrt{x_{ij}^2 + y_{ij}^2}$  and  $\theta_{ij}$  is the angle between the vectors normal to the  
322 planes of the two bases. Similarly to other annotation approaches *Gendron et al.*  
323 (2001); *Sarver et al. (2008)*; *Waleń et al. (2014)*, we identify four different classes  
324 of stacking interactions according to the sign of the  $z$  coordinates:

- 325 • upward: ( $>>$  or 3'-5') if  $z_{ij} > 0$  and  $z_{ji} < 0$
- 326 • downward: ( $<<$  or 5'-3') if  $z_{ij} < 0$  and  $z_{ji} > 0$
- 327 • outward: ( $<>$  or 5'-5') if  $z_{ij} < 0$  and  $z_{ji} < 0$
- 328 • inward: ( $><$  or 3'-3') if  $z_{ij} > 0$  and  $z_{ji} > 0$

329 **Base-pairing.** Base-pairs are classified according to the Leontis-Westhof  
330 nomenclature *Leontis and Westhof (2001)*, based on the observation that hy-  
331 drogen bonding between RNA bases involve three distinct edges: Watson-Crick  
332 (W), Hoogsteen edge (H), and sugar (S). An additional distinction is made accord-  
333 ing to the orientation with respect to the glycosydic bonds, in cis (c) or trans (t)  
334 orientation.

335 In Barnaba, all non-stacked bases are considered base-paired if  $|\theta_{ij}| < 60^\circ$   
336 and there exists at least one hydrogen bond, calculated as the number of donor-  
337 acceptor pairs with distance  $< 3.3\text{\AA}$ . Edges are defined according to the value of  
338 the angle  $\psi = \arctan(\hat{y}_{ij}/\hat{x}_{ij})$ .

- 339 • Watson-Crick edge (W):  $0.16 < \psi \leq 2.0\text{rad}$
- 340 • Hoogsteen edge (H):  $2.0 < \psi \leq 4.0\text{rad}$ .

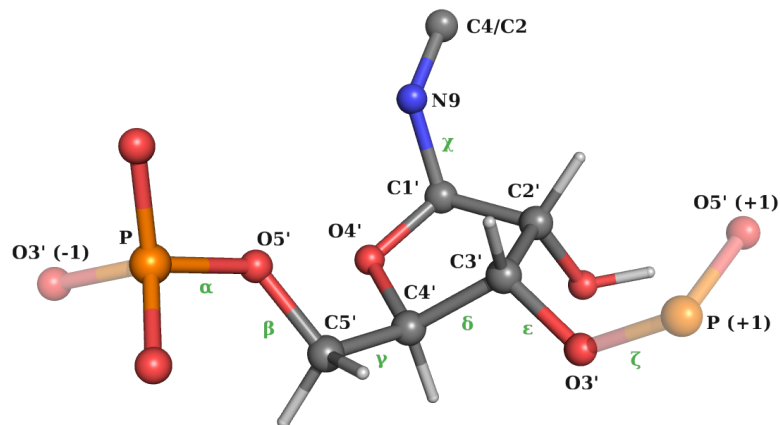


**Figure 8.** Definition of the backbone/glycosidic angles  $\chi$  *Frellsen et al. (2009)*.

- Sugar edge (S):  $\psi > 4.0rad, \psi \leq 0.16rad$

These threshold values are obtained by considering the empirical distribution of base-base interactions shown in Figure 2 in *Bottaro et al. (2014)*. Cis/trans orientation is calculated according to the value of the dihedral angle defined by  $C1'_i - N1/N9_i - N1/N9_j - C1'_j$ , where N1/N9 is used for pyrimidines and purines, respectively.

We note that the annotation provided by Barnaba might fail in detecting some interactions, and sometimes differs from other programs (e.g. X3DNA, MCAAnnotate, Fr3D, etc.). This is due to the fact that for non-Watson-Crick and stacking interactions it is not trivial to define a set of criteria for a rigorous discrete classification *Waleń et al. (2014)*. Typically, these criteria are calibrated to work well for high-resolution structures, but they are not always suitable to describe nearly-formed interactions often observed in molecular simulations.

### Torsion angles and $^3J$ scalar couplings

We use the standard definition of backbone angles, glycosidic  $\chi$  angle (O4'-C1'-N9-C4 atoms for A/G, O4'-C1'-N1-C2 for C/U) and sugar torsion angles ( $v_0 \dots v_4$ ) as shown in Fig.9 *Saenger (2013)*. Pseudorotation sugar parameters amplitude  $tm$  and phase  $P$  are calculated as described in *Altona and Sundaralingam (1972)*

$$P0 = \arctan2(v_4 + v_1 - v_3 - v_0, 3.0777v_2)$$

$$tm = v_2 P0 \quad (5)$$

$$P = \frac{180}{\pi} P0 \quad (6)$$

$$(7)$$



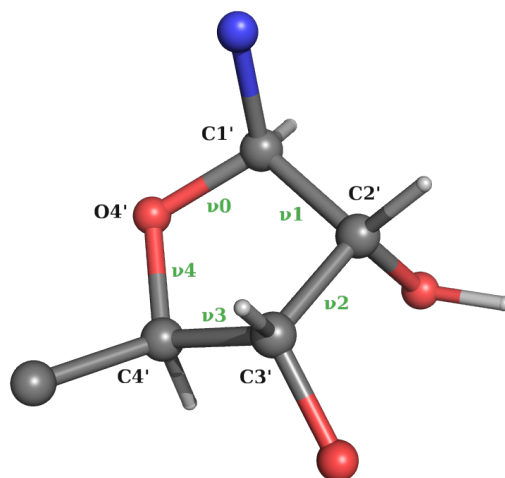


**Figure 9.** Definition of pucker angles  $\nu_0 \dots \nu_4$

359  $^3J$  Scalar couplings are calculated using the Karplus equations

$$A \cos^2(\theta + \phi) + B \cos(\theta + \phi) + C \quad (8)$$

360 Karplus parameters relative to the different scalar couplings are reported in Table  
361 1.

### 362 Elastic Network Model

In ENMs, a set of  $N$  beads connected by pairwise harmonic springs penalize deviations of inter-bead distances from their reference values. Spring constants are set to a constant value  $k$  whenever the reference distance between the two beads is smaller than an interaction cutoff ( $R_c$ ), and set to zero otherwise. Under these assumptions, the potential energy of the system can be approximated as

$$U(\delta r_{i,\mu}, \delta r_{j,\nu}) = \delta r_{i,\mu} \mathbf{M}_{ij,\mu\nu} \delta r_{j,\nu} \quad (9)$$

363 where  $\mathbf{M}$  is the symmetric  $3N \times 3N$  interaction matrix, and  $\delta \mathbf{r}_i$  is the deviation of  
364 bead  $i$  from its position in the reference structure.

365 The user can select different atoms to be used as beads in the construction  
366 of the model. The optimal value of the parameter  $R_c$  depends on this choice, as  
367 described in Ref. *Pinamonti et al. (2015)*.

The covariance matrix is computed as

$$C_{ij,\mu\nu} = \sum_{\alpha=6}^{3N} \frac{1}{\lambda_\alpha} v_{i,\mu}^\alpha v_{j,\nu}^\alpha \quad (10)$$

368 Where  $\lambda_\alpha$  and  $\mathbf{v}^\alpha$  are the eigenvalues and the eigenvectors of the interaction matrix  
369  $\mathbf{M}$ , respectively. The sum on  $\alpha$  runs over all non-null modes of the system.

**Table 1.** Karplus parameters used in Barnaba

Name	$\theta$	A	B	C	$\phi$	Ref
H1'-H2'	H1'-C1'-C2'-H2'	9.67	-2.03	0	0	<i>Condon et al. (2015)</i>
H2'-H3'	H2'-C2'-C3'-H3'	9.67	-2.03	0	0	<i>Condon et al. (2015)</i>
H3'-H4'	H3'-C3'-C4'-H4'	9.67	-2.03	0	0	<i>Condon et al. (2015)</i>
H5'-P	$\beta$	15.3	-6.1	1.6	$-2/3\pi$	<i>Lankhorst et al. (1984)</i>
H5''-P	$\beta$	15.3	-6.1	1.6	$2/3\pi$	<i>Lankhorst et al. (1984)</i>
C4-P	$\beta$	6.9	-3.4	0.7	0.0	<i>Marino et al. (1999)</i>
H4'-H5'	$\gamma$	9.7	-1.8	0.0	$-2/3\pi$	<i>Davies (1978)</i>
H4'-H5''	$\gamma$	9.7	-1.8	0.0	0.0	<i>Davies (1978)</i>
H3-P(+1)	$\epsilon$	15.3	-6.1	1.6	$2/3\pi$	<i>Lankhorst et al. (1984)</i>
C4-P(+1)	$\epsilon$	6.9	-3.4	0.7	0.0	<i>Marino et al. (1999)</i>
H1'-C8/C6	$\chi$	4.5	-0.6	+0.1	$-\pi/3$	<i>Ippel et al. (1996)</i>
H1'-C4/C2	$\chi$	4.7	2.3	0.1	$-\pi/3$	<i>Ippel et al. (1996)</i>

Mean square fluctuation (MSF) of residue  $i$  is calculated as:

$$\text{MSF}_i = \langle \delta r_i^2 \rangle = \sum_{\mu=1}^3 C_{ii,\mu\mu} \quad (11)$$

370 The variance of the distance between two beads can be directly obtained from  
371 the covariance matrix in the linear perturbation regime as

$$\sigma_{d_{ij}}^2 = \sum_{\mu,\nu=1}^3 \frac{\tilde{d}_{ij}^\mu \tilde{d}_{ij}^\nu}{\tilde{d}^2} (C_{ii,\mu\nu} + C_{jj,\mu\nu} - C_{ij,\mu\nu} - C_{ji,\mu\nu}) \quad (12)$$

372 where  $\tilde{d}_{ij}^\mu$  is the  $\mu$  Cartesian component of the reference distance between bead  $i$   
373 and  $j$ .

For most practical applications of ENMs only the high-amplitude modes, i.e. those with the smallest eigenvalues, provide interesting dynamical information. The calculation of C2-C2 distance fluctuations using Eq. 12 requires the knowledge of all eigenvectors. This can be performed by reducing the system to the "effective interaction matrix"  $M_{C2}^{\text{eff}}$  relative to the beads of interest *Zen et al. (2008)*.

$$M = \left( \begin{array}{c|c} M_{C2} & W \\ \hline W^T & M_{\text{other}} \end{array} \right) \quad (13)$$

Where  $M_{C2}$  ( $M_{\text{other}}$ ) is formed by the rows and columns of  $M$  relative to the (non) C2 beads, while  $W$  represent the interactions between C2 and non-C2 beads. The effective interaction matrix is defined as

$$M_{C2}^{\text{eff}} = M_{C2} - W M_{\text{other}}^{-1} W^T \quad (14)$$

374 This can be computed efficiently using sparse matrix-vector multiplication algo-  
375 rithms. The resulting effective matrix  $M_{C2}^{eff}$  has reduced size (1/3 for SBP-ENM,  
376 1/20 for AA-ENM) making its pseudo-inversion considerably faster. Note that, in  
377 case one is interested in computing the C2-C2 fluctuations for a portion of the  
378 molecule only, the algorithm could be further optimized by directly computing  
379 the effective interactions matrix associated to the required C2-C2 pairs.

## 380 Acknowledgments

381 We thank D.E Shaw Research for providing the simulation of the UUCG tetraloop.  
382 The research is funded by a grant from The Velux Foundations (S.B. and K.L.-  
383 L.), a Hallas-Møller Stipend from the Novo Nordisk Foundation (K.L.-L.), and the  
384 Lundbeck Foundation BRAINSTRUC initiative (K.L.-L.). G.B.,S.R, S.B and G.P. have  
385 received funding from the European Research Council (ERC) under the European  
386 Union's Seventh Framework Programme (FP/2007-2013)/ERC grant agreement no.  
387 306662 (S-RNA-S).

## 388 References

- 389 **Abraham MJ**, Murtola T, Schulz R, Páll S, Smith JC, Hess B, Lindahl E. GROMACS: High  
390 performance molecular simulations through multi-level parallelism from laptops to  
391 supercomputers. *SoftwareX*. 2015; 1:19–25.
- 392 **Altona Ct**, Sundaralingam M. Conformational analysis of the sugar ring in nucleosides  
393 and nucleotides. New description using the concept of pseudorotation. *Journal of the*  
394 *American Chemical Society*. 1972; 94(23):8205–8212.
- 395 **Bahar I**, Jernigan RL. Vibrational dynamics of transfer RNAs: comparison of the free and  
396 synthetase-bound forms. *The Journal of Molecular Biology*. 1998; 281(5):871–884.
- 397 **Bottaro S**, Banas P, Sponer J, Bussi G. Free Energy Landscape of GAGA and UUCG RNA  
398 Tetraloops. *J Phys Chem Lett*. 2016; 7(20):4032–4038.
- 399 **Bottaro S**, Bussi G, Kennedy SD, Turner DH, Lindorff-Larsen K. Conformational ensembles  
400 of RNA oligonucleotides from integrating NMR and molecular simulations. *Science*  
401 *Advances*. 2018; 4(5):eaar8521.
- 402 **Bottaro S**, Di Palma F, Bussi G. The role of nucleobase interactions in RNA structure and  
403 dynamics. *Nucleic Acids Res*. 2014; 42(21):13306–13314.
- 404 **Bottaro S**, Lindorff-Larsen K. Mapping the universe of RNA tetraloop folds. *Biophys J*.  
405 2017; 113(2):257–267.
- 406 **Chen H**, Meisburger SP, Pabit SA, Sutton JL, Webb WW, Pollack L. Ionic strength-dependent  
407 persistence lengths of single-stranded RNA and DNA. *Proceedings of the National*  
408 *Academy of Sciences*. 2012; 109(3):799–804.

- 409 **Condon DE**, Kennedy SD, Mort BC, Kierzek R, Yildirim I, Turner DH. Stacking in RNA:  
410 NMR of four tetramers benchmark molecular dynamics. *J Chem Theor Comput*. 2015;  
411 11(6):2729–2742.
- 412 **Davies DB**. Conformations of nucleosides and nucleotides. *Prog Nucl Magn Reson*  
413 *Spectrosc*. 1978; 12(3):135–225.
- 414 **Dickerson R**. Definitions and nomenclature of nucleic acid structure components. *Nucleic*  
415 *acids research*. 1989; 17(5):1797–1803.
- 416 **Ester M**, Kriegel HP, Sander J, Xu X, et al. A density-based algorithm for discovering clusters  
417 in large spatial databases with noise. In: *Kdd*, vol. 96; 1996. p. 226–231.
- 418 **Frellsen J**, Moltke I, Thiim M, Mardia K, Ferkinghoff-Borg J, Hamelryck T. A Probabilistic  
419 Model of RNA Conformational Space. *PLoS Comput Biol*. 2009; 5(3):e1000406.
- 420 **Gendron P**, Lemieux S, Major F. Quantitative analysis of nucleic acid three-dimensional  
421 structures. *Journal of molecular biology*. 2001; 308(5):919–936.
- 422 **Górska A**, Jasiński M, Trylska J. MINT: software to identify motifs and short-range interac-  
423 tions in trajectories of nucleic acids. *Nucleic acids research*. 2015; 43(17):e114–e114.
- 424 **Hajdin CE**, Bellaousov S, Huggins W, Leonard CW, Mathews DH, Weeks KM. Accurate  
425 SHAPE-directed RNA secondary structure modeling, including pseudoknots. *Proc Natl*  
426 *Acad Sci*. 2013; 110(14):5498–5503.
- 427 **Ippel J**, Wijmenga S, De Jong R, Heus H, Hilbers C, De Vroom E, Van der Marel G, Van Boom  
428 J. Heteronuclear scalar couplings in the bases and sugar rings of nucleic acids: their  
429 determination and application in assignment and conformational analysis. *Magn Reson*  
430 *Chem*. 1996; 34(13):S156–S176.
- 431 **Kabsch W**. A solution for the best rotation to relate two sets of vectors. *Acta Crystallo-*  
432 *graphica Section A: Crystal Physics, Diffraction, Theoretical and General Crystallography*.  
433 1976; 32(5):922–923.
- 434 **Kuhrova P**, Best RB, Bottaro S, Bussi G, Sponer J, Otyepka M, Banas P. Computer folding  
435 of RNA tetraloops: identification of key force field deficiencies. *Journal of chemical*  
436 *theory and computation*. 2016; 12(9):4534–4548.
- 437 **Kumar R**, Grubmüller H. do\_x3dna: a tool to analyze structural fluctuations of dsDNA or  
438 dsRNA from molecular dynamics simulations. *Bioinformatics*. 2015; 31(15):2583–2585.
- 439 **Lankhorst PP**, Haasnoot CA, Erkelens C, Altona C. Carbon-13 NMR in conformational  
440 analysis of nucleic acid fragments 2. A reparametrization of the Karplus equation for  
441 vicinal NMR coupling constants in CCOP and HCOP fragments. *J Biomol Struct Dyn*.  
442 1984; 1(6):1387–1405.
- 443 **Lavery R**, Moakher M, Maddocks JH, Petkeviciute D, Zakrzewska K. Conformational  
444 analysis of nucleic acids revisited: Curves+. *Nucleic acids research*. 2009; 37(17):5917–  
445 5929.

- 446 **Leontis NB**, Westhof E. Geometric nomenclature and classification of RNA base pairs.  
447 *Rna*. 2001; 7(4):499–512.
- 448 **Lu XJ**, Bussemaker HJ, Olson WK. DSSR: an integrated software tool for dissecting the  
449 spatial structure of RNA. *Nucleic acids research*. 2015; 43(21):e142–e142.
- 450 **Lu XJ**, Olson WK. 3DNA: a versatile, integrated software system for the analysis, rebuilding  
451 and visualization of three-dimensional nucleic-acid structures. *Nature protocols*. 2008;  
452 3(7):1213–1227.
- 453 **Marino JP**, Schwalbe H, Griesinger C. J-coupling restraints in RNA structure determination.  
454 *Acc Chem Res*. 1999; 32(7):614–623.
- 455 **McGibbon RT**, Beauchamp KA, Harrigan MP, Klein C, Swails JM, Hernández CX, Schwantes  
456 CR, Wang LP, Lane TJ, Pande VS. MDTraj: A Modern Open Library for the Analysis of  
457 Molecular Dynamics Trajectories. *Biophysical Journal*. 2015; 109(8):1528 – 1532. doi:  
458 [10.1016/j.bpj.2015.08.015](https://doi.org/10.1016/j.bpj.2015.08.015).
- 459 **Merino EJ**, Wilkinson KA, Coughlan JL, Weeks KM. RNA structure analysis at single nu-  
460 cleotide resolution by selective 2'-hydroxyl acylation and primer extension (SHAPE).  
461 *Journal of the American Chemical Society*. 2005; 127(12):4223–4231.
- 462 **Michaud-Agrawal N**, Denning EJ, Woolf TB, Beckstein O. MDAnalysis: a toolkit for the  
463 analysis of molecular dynamics simulations. *Journal of computational chemistry*. 2011;  
464 32(10):2319–2327.
- 465 **Nozinovic S**, Fürtig B, Jonker HR, Richter C, Schwalbe H. High-resolution NMR structure of  
466 an RNA model system: the 14-mer cUUCGg tetraloop hairpin RNA. *Nucleic Acids Res*.  
467 2010; 38(2):683–694.
- 468 **Parisien M**, Cruz JA, Westhof É, Major F. New metrics for comparing and assessing  
469 discrepancies between RNA 3D structures and models. *Rna*. 2009; 15(10):1875–1885.
- 470 **Pinamonti G**, Bottaro S, Micheletti C, Bussi G. Elastic network models for RNA: a com-  
471 parative assessment with molecular dynamics and SHAPE experiments. *Nucleic acids  
472 research*. 2015; 43(15):7260–7269.
- 473 **Pinamonti G**, Zhao J, Condon DE, Paul F, Noé F, Turner DH, Bussi G. Predicting the kinetics  
474 of RNA oligonucleotides using Markov state models. *Journal of chemical theory and  
475 computation*. 2017; 13(2):926–934.
- 476 **Richardson JS**, Schneider B, Murray LW, Kapral GJ, Immormino RM, Headd JJ, Richardson  
477 DC, Ham D, HersHKovits E, Williams LD, et al. RNA backbone: consensus all-angle con-  
478 formers and modular string nomenclature (an RNA Ontology Consortium contribution).  
479 *Rna*. 2008; 14(3):465–481.
- 480 **Saenger W**. Principles of nucleic acid structure. Springer Science & Business Media; 2013.
- 481 **Sarver M**, Zirbel CL, Stombaugh J, Mokdad A, Leontis NB. FR3D: finding local and compos-  
482 ite recurrent structural motifs in RNA 3D structures. *Journal of mathematical biology*.  
483 2008; 56(1-2):215–252.

- 484 **Setny P**, Zacharias M. Elastic Network Models of Nucleic Acids Flexibility. *Journal of*  
485 *Chemical Theory and Computation*. 2013; 9(12):5460–5470.
- 486 **Tan D**, Piana S, Dirks RM, Shaw DE. RNA force field with accuracy comparable to state-of-  
487 the-art protein force fields. *Proceedings of the National Academy of Sciences*. 2018; p.  
488 201713027.
- 489 **Tiberti M**, Papaleo E, Bengtsen T, Boomsma W, Lindorff-Larsen K. ENCORE: soft-  
490 ware for quantitative ensemble comparison. *PLoS computational biology*. 2015;  
491 11(10):e1004415.
- 492 **Tirion MM**. Large amplitude elastic motions in proteins from a single-parameter, atomic  
493 analysis. *Phys Rev Lett*. 1996; 77(9):1905.
- 494 **Waleń T**, Chojnowski G, Gierski P, Bujnicki JM. ClaRNA: a classifier of contacts in RNA 3D  
495 structures based on a comparative analysis of various classification schemes. *Nucleic*  
496 *acids research*. 2014; 42(19):e151–e151.
- 497 **Yang C**, Lim M, Kim E, Pak Y. Predicting RNA structures via a simple van der Waals  
498 correction to an all-atom force field. *Journal of chemical theory and computation*. 2017;  
499 13(2):395–399.
- 500 **Zen A**, Carnevale V, Lesk AM, Micheletti C. Correspondences between low-energy modes  
501 in enzymes: Dynamics-based alignment of enzymatic functional families. *Protein*  
502 *Science*. 2008; 17(5):918–929.
- 503 **Zimmermann MT**, Jernigan RL. Elastic network models capture the motions apparent  
504 within ensembles of RNA structures. *RNA*. 2014; 20(6):792–804.